

Gaussian Process-Gated Hierarchical Mixtures of Experts

Yuhao Liu, *Member, IEEE*, Marzieh Ajirak, *Member, IEEE*, and Petar M. Djurić, *Fellow, IEEE*

Abstract—In this paper, we propose novel Gaussian process-gated hierarchical mixtures of experts (GPHMEs) that are used for building gates and experts. Unlike in other mixtures of experts where the gating models are linear to the input, the gating functions of our model are inner nodes built with Gaussian processes based on random features that are non-linear and non-parametric. Further, the experts are also built with Gaussian processes and provide predictions that depend on test data. The optimization of the GPHMEs is carried out by variational inference. There are several advantages of the proposed GPHMEs. One is that they outperform tree-based HME benchmarks that partition the data in the input space. Another advantage is that they achieve good performance with reduced complexity. A third advantage of the GPHMEs is that they provide interpretability of deep Gaussian processes and more generally of deep Bayesian neural networks. Our GPHMEs demonstrate excellent performance for large-scale data sets even with quite modest sizes.

Index Terms—Gaussian processes, mixtures of experts, soft decision trees, random features.



1 INTRODUCTION

IN this paper, we build a hierarchical mixture of experts by way of Gaussian processes (GPs). Models based on hierarchical mixtures of experts (HMEs) have been used in numerous regression, classification, and fusion applications in healthcare, finance, and pattern recognition, [Jordan and Jacobs(1994)]. These models can be viewed as conditional mixture models where distributions of target variables are represented by mixtures of experts, with the experts and the mixing coefficients being conditioned on the input variables. The model parameters are usually estimated by maximizing the likelihood, but this results in severe overfitting. In combating this issue, [Bishop and Svensén(2012)], formulated a fully Bayesian treatment of the model based on variational inference. The authors in [Agrawal and Domke(2021)] also introduced an end-to-end differentiable amortized variational inference algorithm for HMEs and used a recurrent neural network to approximate the posterior distribution over tree node routing decisions.

We observe that the hierarchical mixtures of experts share the same framework of soft decision trees with fixed tree structure. We recall that a decision tree is a hierarchical structure composed of internal decision nodes and terminal leaves [Loh(2011)], [Quinlan(2014)]. A canonical decision tree is composed of internal nodes that represent tests on attributes. Based on the results of the test, the tree assigns samples to one of the children. The leaves on the other hand hold the labels for the classification tasks or are constants for the regression tasks. As a result, a sample traverses a single path from the root to one of the leaves.

The nodes can be univariate, which entails that they use only one feature of the input and compare it against a threshold value [Quinlan(2014)]. If they are multivariate nodes, they define a linear discriminant in the input space that is used for comparisons [Murthy et al.(1994)Murthy, Kasif, and Salzberg], [Yildiz and Alpaydin(2005)]. This discriminant can be generalized to be nonlinear [Guo and Gelfand(1992)]. Trees can have any kind of nodes chosen

by a statistical model selection procedure [Yildiz and Alpaydin(2001)].

Unlike in hard deterministic trees, in soft probabilistic decision trees, all the children are selected with a certain probability, [Irsoy et al.(2012)Irsoy, Yıldız, and Alpaydin]. Namely, all the possible paths to all the leaves are traversed and the final decision is contributed by all the leaves but with different probabilities. Gaussian soft decision trees for interpretable feature-based classification were studied in [Yoo and Sael(2021)]. In [Frosst and Hinton(2017)], a deep neural network (DNN) was used to train a soft decision tree that mimics the input-output function discovered by a neural network (NN). The authors use soft decision trees in order to provide interpretability for DNNs and explainability of the representations of individual hidden layers. They are equivalent to a hierarchical mixture of experts with parametric probabilistic tree-based aggregation [Jordan and Jacobs(1994)]. The experts are the leaves, while the coefficients are obtained by the gating nodes.

GP extensions to HMEs have also been studied, [Shi et al.(2005)Shi, Murray-Smith, and Titterton], [Ng and Deisenroth(2014)]. Further, [Lawrence and Moore(2007)], investigated the unsupervised case in hierarchical GP latent variable models. We observe that the GP-based HME models rely mostly on function spaces rather than feature spaces.

Sparse GPs reduce the complexity of standard GPs from cubic to quadratic. There are two main approaches for reducing the complexity: the inducing point-based approach and the random feature (RF)-based approach. Unlike inducing point-based methods, the random feature framework does not require any matrix decomposition, and instead, it only needs matrix products, which in turn boosts its speed significantly. Random feature-based GPs transform nonlinear input spaces into linear kernel feature spaces (hereinafter called feature spaces to distinguish from the input spaces). Several papers have pointed out the connection between GPs and NNs, [Lee et al.(2017)Lee, Bahri, Novak,

Schoenholz, Pennington, and Sohl-Dickstein], [Wilson and Izmailov(2020)], [Dutordoir et al.(2021)Dutordoir, Hensman, van der Wilk, Ek, Ghahramani, and Durrande], [Pleiss and Cunningham(2021)]. Given the relationship between the GPs and single-layered NNs with an infinite number of hidden units [Neal(2012)], GPs alleviate the issue of specifying the number of units in hidden layers by implicitly working with infinite representations. In view of feature spaces, GP models yield Bayesian neural networks (BNNs) that quantify uncertainties.

One approximation of GPs with feature spaces takes advantage of random Fourier features. Random Fourier features for large-scale kernel machines were proposed in [Rahimi and Recht(2007)] and applications of random features to GPs were studied in [Lázaro-Gredilla et al.(2010)Lázaro-Gredilla, Quinonero-Candela, Rasmussen, and Figueiras-Vidal]. Variational learning of the posterior over the frequencies when the squared exponential kernel is used was proposed in [Gal and Turner(2015)]. The RF expansion for different kernels of GPs results in different activation functions of NNs, for instance, trigonometric for the Radial Basis Function (RBF) kernel, and Rectified Linear Unit (ReLU) functions for the ARC-COSINE kernel.

The above models, however, partition the data only in the input space, either in the form of HMEs or soft decision trees. In other words, the gating models or the inner nodes are linear functions of the inputs. In this paper, we propose GP-gated HMEs (GPHMEs) with structures of fixed complete binary trees where both, the gating and expert models, rely on RF expansions of GPs. This allows for making decisions by the GPs in linear feature spaces and for a considerable reduction of complexity of the trees. We optimize the GPHMEs by using variational inference and by exploiting the reparameterization trick. In practice, the results show that the optimal height of a tree is no greater than four even for large-scale data sets with more than millions of samples. The smaller size of our tree structure is a result of the nonlinear transformation of the input space and the oblique decision mechanisms that are created. Further, the GPHME outperforms the tree-based benchmarks that partition the input data.

Our model can also be used in providing interpretability of deep GPs (DGPs). DGPs are deep belief networks based on a stack of GP mappings, where each hidden layer is composed of a multivariate GP. In practice, DGPs require less depth and width compared to DNNs. However, the DGPs encounter the problem of interpreting the hidden layers. Similar to the interpretability of DNNs distilled by soft decision trees [Frosst and Hinton(2017)], this paper provides ways of getting insights into understanding how a DGP makes its decisions.

In summary, the contributions of this paper are as follows: (i) we propose a novel HME, GPHME, that relies on RF-based GPs; (ii) we demonstrate the ability of our work to outperform related state-of-the-art methods, including HMEs, decision trees, and GP-based models. Further, the proposed GPHME has reduced complexity and is readily applicable to large-scale problems; (iii) we quantify the uncertainty of probability distributions offered by GPs compared to trees; (iv) we provide an explainable way for interpreting the behaviors of DGPs.

2 BACKGROUND

A GP is a stochastic process (a collection of random variables indexed by time or space), such that every finite collection of these random variables has a multivariate normal distribution. More specifically, for a finite set of inputs $\mathbf{X} \in \mathbb{R}^{N \times D_x}$, where N is the number of inputs and D_x is the dimension of the input, the corresponding outputs $\mathbf{y} \in \mathbb{R}^N$ follow a Gaussian process f , where $f(\mathbf{X}) \sim \mathcal{N}(\mathbf{0}, \kappa(\mathbf{X}, \mathbf{X}))$, with $\kappa(\cdot, \cdot)$ being a kernel or covariance function. A popular example of a stationary kernel is the Radial Basis Function (RBF) defined by

$$\kappa(\mathbf{x}, \mathbf{x}') = \sigma_\lambda^2 \bar{\kappa}(\mathbf{x}, \mathbf{x}') = \sigma_\lambda^2 \exp \left[-\frac{1}{2} \sum_{d=1}^{D_x} \frac{(x_d - x'_d)^2}{\lambda_d^2} \right], \quad (1)$$

where σ_λ^2 is the kernel variance, λ_d is the kernel lengthscale, and $\bar{\kappa}$ is the standardized kernel with norm $\|\bar{\kappa}(\cdot, \cdot)\| \leq 1$.

Another commonly used kernel is the ARC-COSINE kernel with a degree n

$$\tilde{\kappa}(\mathbf{x}, \mathbf{x}') = \frac{\|\mathbf{x}\| \times \|\mathbf{x}'\|}{\pi} J_n(\alpha), \quad (2)$$

where

$$J_n(\alpha) = (-1)^n (\sin \alpha)^{2n+1} \left(\frac{1}{\sin \alpha} \frac{\partial}{\partial \alpha} \right)^n \left(\frac{\pi - \alpha}{\sin \alpha} \right), \quad (3)$$

and

$$\alpha = \cos^{-1} \left(\frac{\mathbf{x}^\top \mathbf{x}'}{\|\mathbf{x}\| \|\mathbf{x}'\|} \right). \quad (4)$$

This kernel is referred to as an arc-cosine kernel because of its dependence on the angle α and the arc-cosine function. In the paper, we use $n = 1$ because it produces ReLU random features, and

$$J_1(\alpha) = \sin \alpha + (\pi - \alpha) \cos \alpha. \quad (5)$$

This kernel can also implement automated relevance determination (ARD) by dividing x_d with λ_d .

2.1 Random Feature Expansions for Gaussian processes

Bochner's theorem states that if $\bar{\kappa}(\mathbf{x}_i, \mathbf{x}_j) = \bar{\kappa}(\mathbf{x}_i - \mathbf{x}_j)$ is a continuous shift-invariant normalized covariance function, it can be rewritten as the Fourier transform of a non-negative measure $p(\boldsymbol{\omega})$ [Rahimi and Recht(2007)]. Let $\boldsymbol{\omega}$ represent a vector of spectral frequencies, $i = \sqrt{-1}$, and $\boldsymbol{\Delta} = \mathbf{x}_i - \mathbf{x}_j$. Then we can write

$$\bar{\kappa}(\boldsymbol{\Delta}) = \int p(\boldsymbol{\omega}) \exp(i \boldsymbol{\Delta}^\top \boldsymbol{\omega}) d\boldsymbol{\omega}, \quad (6)$$

where $p(\boldsymbol{\omega})$ is the Fourier transform of $\bar{\kappa}(\mathbf{x}_i, \mathbf{x}_j)$. We drop the complex part of the argument of the expectation because the covariance function and the nonnegative measures are real, and we keep $\cos(\boldsymbol{\Delta}^\top \boldsymbol{\omega}) = \cos((\mathbf{x} - \mathbf{x}')^\top \boldsymbol{\omega})$, which can also be expressed as $\cos(\mathbf{x}^\top \boldsymbol{\omega}) \cos(\mathbf{x}'^\top \boldsymbol{\omega}) + \sin(\mathbf{x}^\top \boldsymbol{\omega}) \sin(\mathbf{x}'^\top \boldsymbol{\omega})$. Next, we note that with the above expansion we can estimate $\bar{\kappa}(\mathbf{x}, \mathbf{x}')$ using Monte Carlo sampling. If $\mathbf{z}(\mathbf{x}, \boldsymbol{\omega}) = [\cos(\mathbf{x}^\top \boldsymbol{\omega}), \sin(\mathbf{x}^\top \boldsymbol{\omega})]$, an unbiased estimate of $\bar{\kappa}(\mathbf{x}, \mathbf{x}')$ can be obtained by

$$\bar{\kappa}(\mathbf{x}, \mathbf{x}') \approx \frac{1}{J} \sum_{j=1}^J \mathbf{z}(\mathbf{x}, \boldsymbol{\omega}_j) \mathbf{z}(\mathbf{x}', \boldsymbol{\omega}_j)^\top, \quad (7)$$

where the ω_j s are samples from $p(\omega)$, and J is the number of random samples of spectral frequencies. Using \mathbf{x} and the random samples ω_j , which are columns of Ω , and where $\Omega \in \mathbb{R}^{D_x \times J}$ (or, $\Omega_{\cdot j} = \omega_j$), we define the random features for the RBF kernel by

$$\phi(\mathbf{x}) \triangleq \frac{\sigma_\lambda}{\sqrt{J}} [\sin(\mathbf{x}^\top \Omega), \cos(\mathbf{x}^\top \Omega)]^\top,$$

where

$$\sin(\mathbf{x}^\top \Omega) = \left[\sin(\mathbf{x}^\top \omega_1) \quad \sin(\mathbf{x}^\top \omega_2) \quad \dots \quad \sin(\mathbf{x}^\top \omega_J) \right]. \quad (8)$$

The definition of $\cos(\mathbf{x}^\top \Omega)$ is analogous. Following [Cho and Saul(2009)], an integral representation of the ARC-COSINE kernel is given by

$$\begin{aligned} \tilde{\kappa}(\mathbf{x}, \mathbf{x}') \\ = 2 \int \mathbf{x}^\top \omega \omega^\top \mathbf{x}' H(\omega^\top \mathbf{x}) H(\omega^\top \mathbf{x}') \mathcal{N}(\omega | \mathbf{0}, \mathbf{I}) d\omega, \end{aligned} \quad (9)$$

where $H(\cdot)$ is the Heaviside function. Similarly to the RBF kernel, the random feature based on this covariance leads to

$$\phi(\mathbf{x}) \triangleq \frac{\sqrt{2}\sigma_\lambda}{\sqrt{J}} \max(\mathbf{0}, \Omega^\top \mathbf{x}). \quad (10)$$

We note that the identity feature is defined by

$$\phi(\mathbf{x}) \triangleq [1 \ \mathbf{x}^\top]^\top. \quad (11)$$

Our model reduces to an ordinary Bayesian HME when we take the feature space from (11). Therefore, we express the different approximation of the kernels by $k(\mathbf{x}, \mathbf{x}') = \phi(\mathbf{x})^\top \phi(\mathbf{x}')$, and we define the GP approximation of f by

$$\hat{f}(\mathbf{x}) = \phi(\mathbf{x})^\top \mathbf{w}, \quad (12)$$

where the weight \mathbf{w} is a parameter vector with a Gaussian prior, $\mathcal{N}(\mathbf{0}, \mathbf{I})$.

3 GAUSSIAN PROCESS-GATED HIERARCHICAL MIXTURES OF EXPERTS

Here we propose GP-gated HMEs (GPHMEs) trained with mini-batch gradient descent to build mixtures of experts. An example of a GPHME is shown in Fig. 1. Each inner node ν of the tree has a learned filter \mathbf{w}_ν and a random vector Ω_ν , whereas each leaf node l has a learned distribution Q_l . At each inner node, the probability of taking the leftmost branch is $\sigma(z_\nu)$. The variable z_ν is defined by

$$z_\nu(\mathbf{x}) = \phi(\mathbf{x}^\top \Omega_\nu) \mathbf{w}_\nu, \quad (13)$$

where \mathbf{x} is the input to the model, and ϕ is the random feature. The equation (13) gives a nonlinear partition of the input space.

The model described by Fig. 1 is a hierarchical mixture of experts and learns a hierarchy of filters that are used to assign each sample to the GP experts with respective path probabilities. Unlike in [Frosst and Hinton(2017)], where each expert is actually a ‘‘bigot’’ because it does not use the test data to compute the experts’ probability distributions,

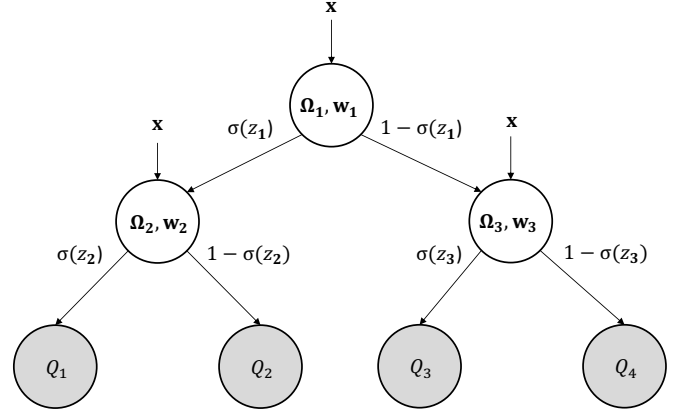


Figure 1. A GPHME with a fixed tree structure, comprising expert leaves, shown as shaded circles and inner nodes, shown as circles. Therefore, the GPHMEs are tree-structured models. The edges represent RF-based decision rules associated with the inner nodes, and the Q s denote the conditional distributions over the target variable y .

the experts in our model learn their distributions over the possible output classes given a test input \mathbf{x} according to

$$Q_l^k = \frac{\exp(z_l^k)}{\sum_{k'} \exp(z_l^{k'})}, \quad (14)$$

where each $z_l^k = \phi(\mathbf{x}^\top \Omega_l) \mathbf{w}_l^k$ is a learned distribution for class k at the l th leaf, and Q_l^k denotes the distribution of probability at that leaf. The objective function, the mixture log-likelihood of Θ for an input-output pair (\mathbf{x}, y) , is defined by

$$\log p(y|\mathbf{x}, \Theta) = \sum_l P(l|\mathbf{x}, \Theta) \log p(y|\mathbf{x}, l, \Theta), \quad (15)$$

where $P(l|\mathbf{x}, \Theta)$ is the probability of arriving at leaf node l given the input \mathbf{x} and Θ , and $p(y|\mathbf{x}, l, \Theta) = Q_l^y$ is the likelihood of Θ of the l th expert. We collectively denote the hidden variables by $\Theta = \{\mathbf{w}_\nu, \mathbf{w}_l^k, \Omega_\nu, \Omega_l\}$, where the index ν refers to the inner nodes and l to the leaf nodes. For multivariate regression tasks, the leaves provide regressors simply by $Q_l^k = z_l^k$, where k refers to the dimension of the multivariate \mathbf{y} . We reiterate that the model is by nature a hierarchical mixture of GP experts, where we project the input \mathbf{x} into different feature spaces to assign paths from the root to the leaves and predict the target distribution at the leaves.

The objective function in (15), however, would encourage each leaf to minimize its log-likelihood, which in turn would lead each leaf to be an expert on all the classes and would result in no preference for any of the classes. In other words, the experts would become jacks of all trades. Although this objective function can help us obtain more accurate results, we may wish that each leaf prefers a specific class to make the tree more interpretable. Therefore, another option of the objective function is the normalized likelihood. Let

$$\log Q^k = \sum_l P(l|\mathbf{x}, \Theta) \log p(k|\mathbf{x}, l, \Theta), \quad (16)$$

be proportional to the log-probability distribution of class k given \mathbf{x} . Specifically, (15) is equivalent to $\log Q^y$, and the normalized likelihood is defined by

$$\text{Normalized Likelihood} = \frac{Q^y}{\sum_k Q^k}. \quad (17)$$

In other words, we not only maximize the likelihood of a class y but also consider the likelihood of y relative to other classes. Consequently, each expert would prefer one class after training, i.e., recognize one specific class with a higher probability on average with respect to other classes. We refer to the objective function in (15) as objective function one (OF1) while to the objective function in (17), as objective function two (OF2). We note that multiple experts might be experts for one class and that they are trained automatically.

4 VARIATIONAL INFERENCE

Our goal is to find a variational distribution $q(\Theta)$ that approximates the true posterior distribution $p(\Theta|\mathbf{X}, \mathbf{Y})$. Defining the marginalized log-likelihood $L = \sum_{n=1}^N \log p(y|\mathbf{x}_n)$ and $L' = \sum_{n=1}^N \mathbb{E}_{q(\Theta)} \log p(y|\mathbf{x}_n, \Theta)$, we have

$$L \geq L' - \text{KL}[q(\Theta)||p(\Theta)], \quad (18)$$

where KL stands for the Kullback-Leibler divergence, and $p(\Theta)$ is the prior distribution of the hidden variables Θ . More specifically,

$$p(\Theta) = \prod_{\nu} \left[p(\mathbf{w}_{\nu}) \prod_j p(\omega_{\nu j}) \right]. \quad (19)$$

Note that the KL divergence regularizes Θ automatically, which avoids overfitting when $\|\mathbf{w}_{\nu}\|$ is too large.

We assume a Gaussian approximating distribution that factorizes across nodes. Then we have

$$q(w_{\nu j}) \sim \mathcal{N}(m_{\nu j}, (s_{\nu j})^2), \quad (20)$$

$$q(\Omega_{\nu ij}) \sim \mathcal{N}(\mu_{\nu ij}, (\sigma_{\nu ij})^2), \quad (21)$$

where $w_{\nu j}$ represents the j th element of \mathbf{w}_{ν} , $\Omega_{\nu ij}$ is the element of Ω_{ν} from the i th row and the j th column. The variational parameters are the mean and the variance of each of the approximating factors $m_{\nu j}$, $s_{\nu j}$, $\mu_{\nu ij}$, and $\sigma_{\nu ij}$, and we aim to optimize the lower bound with respect to these parameters. The settings of the inner nodes \mathbf{w}_{ν} and Ω_{ν} are analogous to the leaves, \mathbf{w}_l^k and Ω_l . Because of the independent observations, we use a doubly-stochastic approximation of L' . If we randomly select M points indexed by \mathcal{I}_M , L' can be estimated in an unbiased way using mini-batches by

$$L' = \frac{N}{M} \sum_{m \in \mathcal{I}_M} \mathbb{E}_{q(\Theta)} L(y_m | \mathbf{x}_m, \Theta). \quad (22)$$

To deal with the expectation term, we resort to Monte Carlo sampling, which yields

$$L' = \frac{N}{M} \sum_{m \in \mathcal{I}_M} \frac{1}{N_{MC}} \sum_{r=1}^{N_{MC}} L(y_m | \mathbf{x}_m, \Theta_r), \quad (23)$$

where Θ_r is sampled from $q(\Theta)$, and N_{MC} is the number of drawn samples. In order to utilize the backward propagation, we apply the reparameterization trick so that the weights are reparameterized as follows:

$$w_{\nu jr} = m_{\nu jr} + s_{\nu jr} \epsilon_{\nu jr}, \quad (24)$$

$$\Omega_{\nu ijr} = \mu_{\nu ijr} + \sigma_{\nu ijr} \epsilon_{\nu ijr}, \quad (25)$$

where the $\epsilon_{\nu jr}$ s and $\epsilon_{\nu ijr}$ s are independent samples from the standard normal distribution. One can also assign prior distributions to σ_{λ} and λ_d and then use variational inference.

In the implementation of gradient descent, the probabilities $\sigma(z_{\nu})$ of the inner nodes are close to 0 or 1 so that the tree tends to assign almost all the probability to one of its branches. To overcome this, we adopt a regularizer defined by the average probability that \mathbf{x} at node ν goes to the left child, and it is given by [Frost and Hinton(2017)],

$$\alpha_{\nu} = \frac{\sum_{\mathbf{x}} P_{\nu}(\mathbf{x}) p_{\nu}(\mathbf{x})}{\sum_{\mathbf{x}} P_{\nu}(\mathbf{x})}, \quad (26)$$

where $P_{\nu}(\mathbf{x}) = P(\nu|\mathbf{x}, \Theta)$ is the probability that \mathbf{x} arrives at node ν and $p_{\nu}(\mathbf{x})$ is the probability that \mathbf{x} goes to the left child of node ν . Therefore, the penalty term becomes

$$C = \lambda N \sum_{\nu} [0.5 \log(\alpha_{\nu}) + 0.5 \log(1 - \alpha_{\nu})], \quad (27)$$

where λ is a hyper-parameter and set to 2^{-d} in our experiments. The penalized evidence lower bound (PELBO) is given by

$$PELBO = L' + C - \text{KL}[q(\Theta)||p(\Theta)]. \quad (28)$$

So far, we set Ω_{ν} to be different at the different nodes, i.e., the random feature spaces are unique for each node (NIS-N), and therefore, they are non-isotropic. However, this might not be necessary and could incur huge costs in space complexity. We could expect that there exists a specific random feature space that separates data linearly, which means that all the nodes share a common distribution of Ω . We refer to this option as the isotropic space of all the nodes (ISO-N). Another option is to restrict the nodes at each level and have them share the same distribution of Ω and thereby mitigating the computation burden. We refer to this as the isotropy of the spaces across the nodes on the same levels (ISO-L). However, this arrangement does not seem reasonable because it is difficult to justify pooling nodes from the same level that are far away from each other. In the section on numerical experiments, the results did show that this option is worse than the other options most of the time. In practice, the ISO-N option is slightly worse than NIS-N. However, despite the slightly worse performance, the ISO-N option provides better interpretability than the NIS-N option on account of the single projected feature space.

The two main operations of inference come from Eqs. (13) and (14). For a mini batch with size M , the computational complexity of (13) is $\mathcal{O}(M J D_x N_{MC}) + \mathcal{O}(M J N_{MC})$, and of (14), $\mathcal{O}(M J D_x N_{MC}) + \mathcal{O}(M J D_y N_{MC})$. Combined with the height of the tree h , the final training complexity is $\mathcal{O}(2^h M J N_{MC} (D_x + D_y))$. The test complexity is $\mathcal{O}(2^h N_{test} J N_{MC} (D_x + D_y))$, where N_{test} is the size of the test set.

The code for obtaining the results in this paper is available at Github.¹

5 NUMERICAL EXPERIMENTS

In this section, we first show how our GPHME explains the DGPs by mimicking their behaviors. Then we discuss the different settings of Ω and choices of the height of trees. Next, we compare our methods with the Bayesian HMEs (BHMEs) [Bishop and Svensén(2012)] as well as with soft and hard trees. All the results suggest that there is a need for projection in feature spaces. Finally, we show results of implementation of our methods on large-scale data.

All the experiments ran on a single machine of NVIDIA TITAN RTX GPU having 24GB RAM, but can also be directly launched on CPUs.

5.1 Explaining DGPs and DNNs with GPHMEs

Each hidden layer of the random feature-based DGP models is in fact a special case of a two-layer BNN, and thus, our GPHMEs explain how the DGPs or more general Bayesian DNNs work. Figure 2 illustrates how our method makes decisions on the MNIST data. If we take, for example, the left-most four leaves, we can see that the most likely classifications are 4 and 9, and therefore, their parent node is simply learning to distinguish between these two digits. This makes sense for groups 4 and 9 because they both have closed regions in their digits. Further, 2 and 5 are the most challenging for classification because none of the experts seem to reach high enough probabilities for confident decisions. The decisions of the inner nodes are made similarly and can readily be understood.

Given the good interpretability in hand, during training, our model achieves the highest accuracy of 97.79% with a tree of height four and with an ISO-N setting. If we use the loss function in (15), we obtain 98.49%, still under an ISO-N setting. With more parameters, the DGP model only peaks at 98.04% when the number of hidden layers is one and decreases with the number of layers increasing. Our GPHME model is also comparable with a one-hidden-layer DNN, which achieves 98.4% accuracy [Simard et al.(2003)Simard, Steinkraus, and Platt]. The GPHME has this accuracy with only two-thirds of the number of parameters of the DNNs. Further, the GPHME attains 98.67% accuracy at most with a height of only two under the NIS-N setting, which is comparable to 98.6% reported by SVMs [Schölkopf(1997)]. It is also better than other kernel-based methods including GPs and their variants [Hensman et al.(2015)Hensman, Matthews, and Ghahramani], [Krauth et al.(2016)Krauth, Bonilla, Cutajar, and Filippone].

5.2 Discussion on hyperparameters

Our tree-based model, due to the information embedded in the feature spaces, does not need to grow the tree too deep. Therefore, in this section, the heights of the trees are chosen up to two. We took one regression data set *Protein* and one multi-output classification data set *Optical Digits* (OPT) from the UCI repository.² The dimension of the random

features was set to 100 for the RBF and the ARC-COSINE kernels. Figure 4 shows the performance under different settings, including different heights of trees, structures of Ω , and kernel types. Without loss of generality and making the figures readable, we only present the results of different structures of Ω when the height of trees equals two.

Figure 3 demonstrates how the models work with different heights of trees and Ω options. The figure also provides results under different Ω options when the height of the tree is one.

As we expected, the performance does not always improve when the height of trees grows because of overfitting. For the setting of Ω , the NIS-N option has the most number of parameters but does not improve the results significantly compared with the ISO-L and the ISO-N options. The ISO-N option beats the NIS-N option in some cases. This is one reason why we prefer the ISO-N option in practice. The ISO-L option is not stable and might obtain the worst results among all of the Ω settings. This is reasonable because this option forces the nodes at the same level to share the common feature spaces. As for the kernel choice, the RBF kernel has better performance in general, while the ARC-COSINE kernel may work better in binary classification tasks. The identity features are discussed in the next section as a benchmark model.

5.3 UCI Data Sets

To compare the generalization error and model complexity of tree-based models, including linear discriminant trees (LDT), hard tree (C4.5), soft tree, and BHMEs, we used the same data sets as in [Irsoy et al.(2012)Irsoy, Yıldız, and Alpaydın], which reported results for LDT, C4.5, and soft-decision trees. However, some data sets cannot be found at this time. Therefore, we only selected those that still exist, including four regression data sets (ABAlone, ADD10, BOSton, CONcrete), eight binary classification data sets (BREast, GERman, MAGic, MUSk2, PIMa, RINGnorm, SPAmbase, TWONorm), and ten multi-class classification data sets (BALance, CMC, DERmatology, ECOli, GLAss, OPTdigits, PAGEblock, PENdigits, SEGment, YEAsT) from the UCI repository. The benchmark methods use five folds of data and then average the results where one-third of the data are test data and the other two-thirds are training data. We adopted the same setting here and still let the height of the trees be at most two for our models. To compare with the BHMEs fairly, we let the height of trees for BHMEs to be large enough so that the number of parameters of BHMEs is just larger than that of our models. In this case, the highest height of trees for BHMEs was usually 7 or 8 on average, although the BHMEs achieve the best results almost always with heights two or three. Besides, we provided the standard deviation across the five shuffled folds while the benchmarks of decision trees did not report this in their source. The results are selected from the best model among different heights and kernel types.

Tables 1, 2, and 3 show the MSEs of regression, the accuracy of binary classification, and accuracy of multi-classification. The tables also include the number of samples N , the dimension of inputs D_x , and the dimension of outputs D_y . The averaged training times over five different

1. <https://github.com/yuhaoliu94/GPHME>.

2. <https://archive.ics.uci.edu>

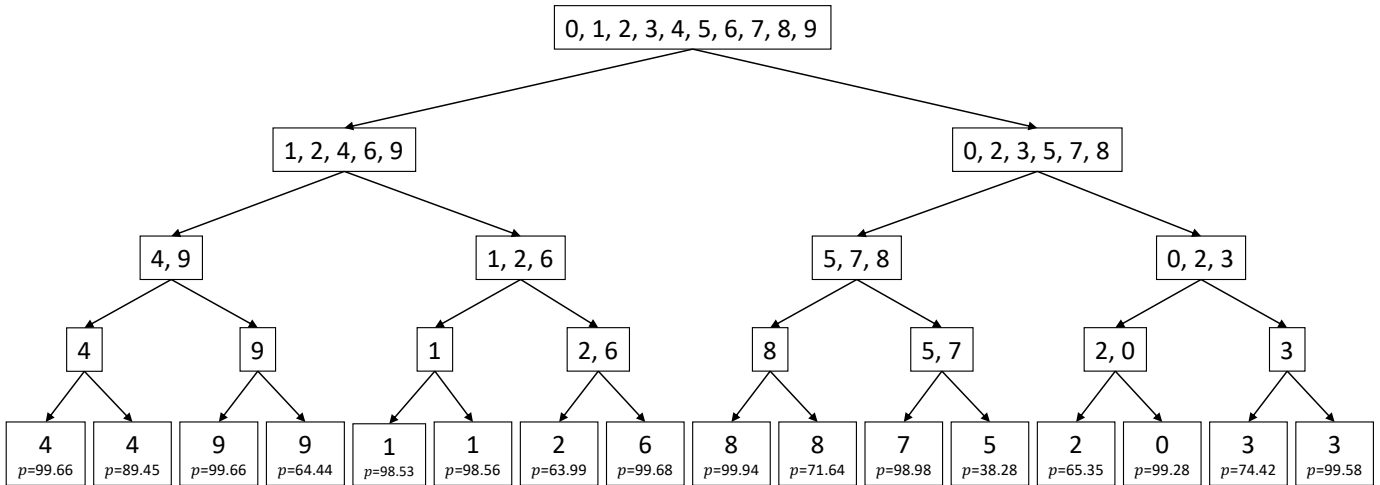


Figure 2. A visualization of a GPHME of depth four trained on the MNIST data set. The final most likely classifications are shown at each leaf with its average probability over samples. The classes annotated at each inner node are traced backward from the leaves to the root. A leaf does not only predict one class but predicts all the classes. If for example, there are 100 samples and a certain leaf predicts 80 of them as digit 0 while 20 of them as any digit from 1-9, then the leaf in the figure is annotated as digit 0 with $p=0.8$. The classes written in the inner nodes are sourced from the leaves backward layer by layer because the predictions occur at the leaves. Our model is a “soft” decision tree, and the paths have probabilities, which entails that a digit could “go” both left and right.

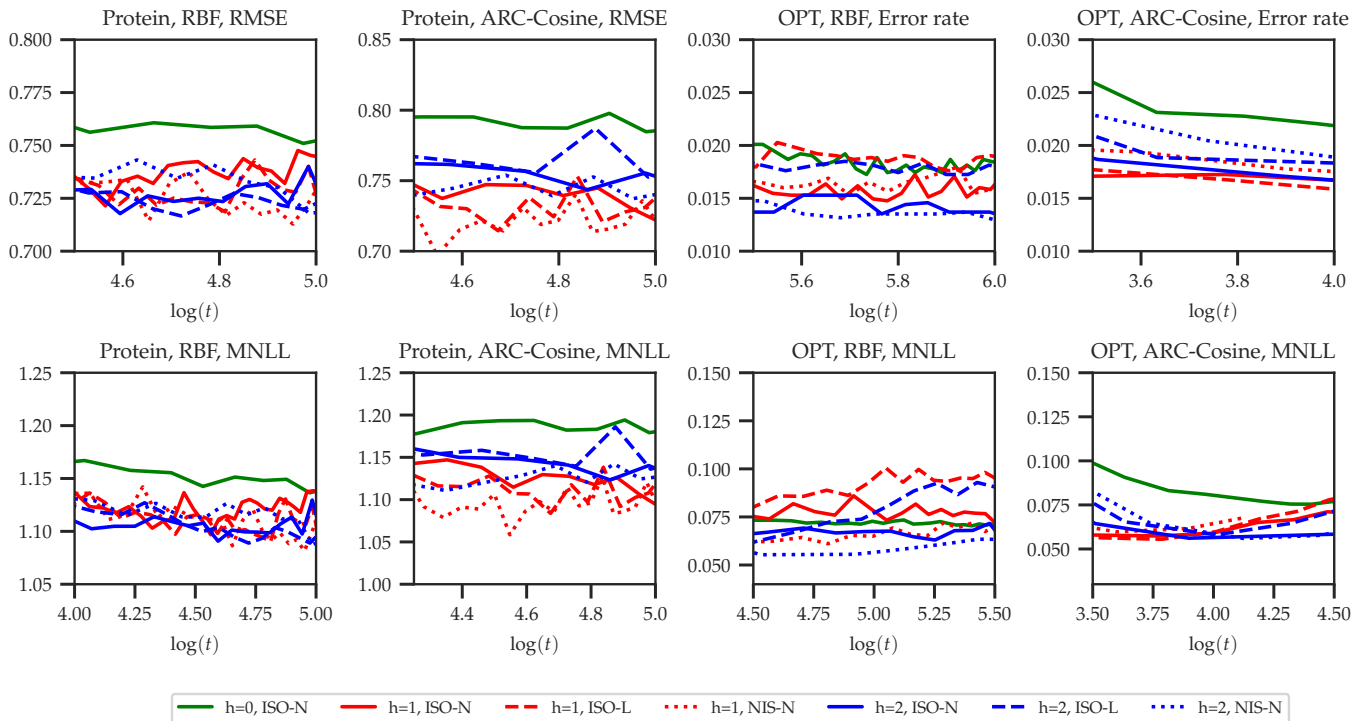


Figure 3. Evolution of RMSE in the regression case, error rate in the classification case, and mean negative log-likelihood (MNLL) over time.

folds for all data sets are also listed. The time duration for the training process was set not to be larger than 60 minutes. The sizes of the applied trees were specified by the numbers of all the inner nodes and leaves. The results of other tree-based benchmarks include C4.5, which corresponds to the univariate hard tree as well as LDT, which is an oblique multivariate hard tree. From the results, it is clear that our model outperforms all the other candidate tree-based models in terms of loss. For example, for the RIN data set, the accuracy of the BHME candidates is only

around 77%, while our model improves it to over 98% for the same size of trees. Further, our tree is smaller in size than the benchmark trees in about 80% of the cases. We applied the unequal variance (Welch) t-test between GPHME and BHME. We did not include the ordinary decision tree models [Irsoy et al.(2014)Irsoy, Yildiz, and Alpaydin] in the Welch t-tests because the variances of their estimates are not provided. The results shown in bold in Tables 1, 2, and 3 are the instances where our method was significantly better. The benchmark results are of trees

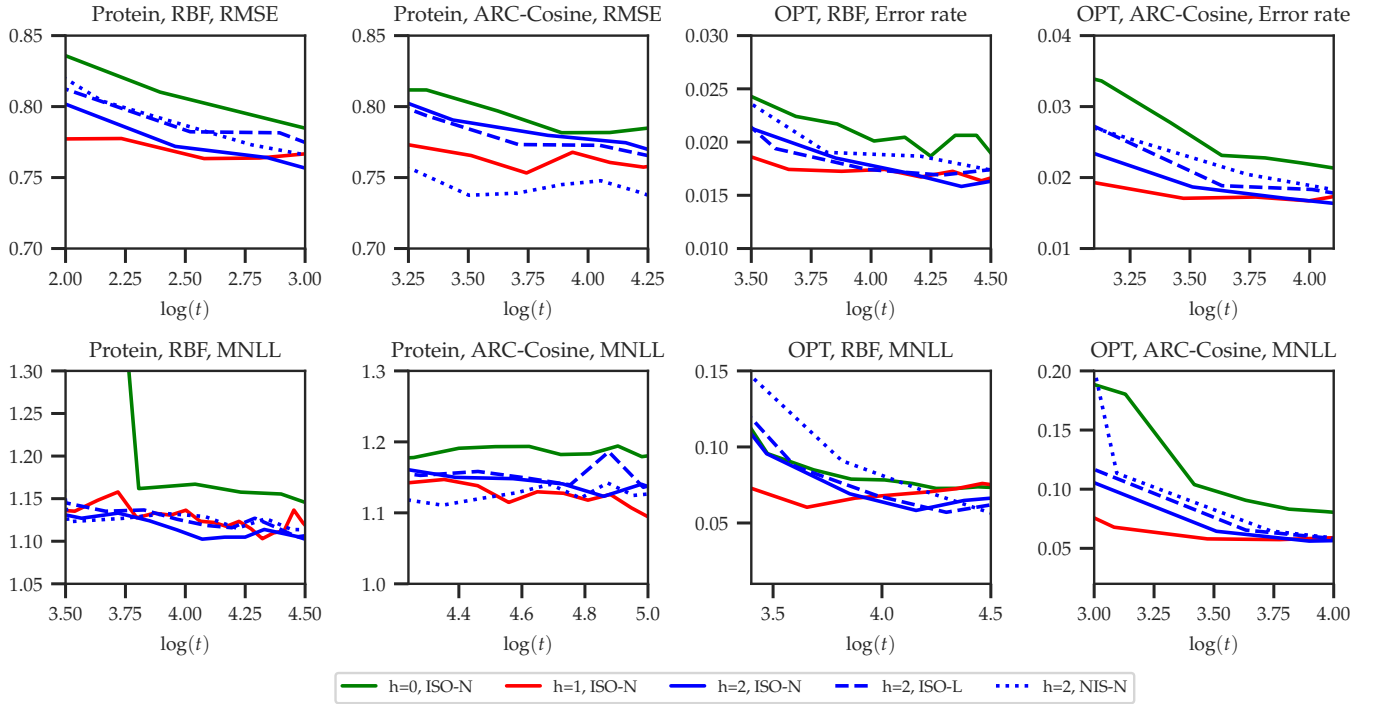


Figure 4. Evolution of RMSEs in the regression case, error rates in the classification case, and mean negative log-likelihood (MNLL) over time. The x-axes of the MNLL panels are different from those of the RMSE and ER panels because the MNLLs converge later than the RMSEs and ERs.

reported in [Irsoy et al.(2012)Irsoy, Yıldız, and Alpaydın], [Irsoy et al.(2014)Irsoy, Yildiz, and Alpaydın]. However, the authors of these papers did not provide variances of the estimates.

5.4 Large-Scale Data Sets

As we mentioned, the GPHMEs can be treated as weak learners and can provide interpretability for DGPs or more generally, Bayesian DNNs. We did not expect our model to perform better than DGPs but were only interested in using them to explain DGPs. However, we were surprised that our model outperformed (at least slightly) the DGPs for most of the time. Moreover, one of the defining characteristics of our model is the ability to scale up to large data sets.

We evaluated our model on two large-scale problems which go beyond the scale of data sets to which GPs and especially DGPs are typically applied. We first considered MNIST8M, which artificially extends the original MNIST data set to 8+ million observations. We trained this model using the same configuration described for standard MNIST with the height of trees as two but with the NIS-N setting. We obtained 99.30% accuracy and 0.0372 MNLL on the test set. These results beat the DGP counterpart provided by [Cutajar et al.(2017)Cutajar, Bonilla, Michiardi, and Filippone]. We would like to point out that the number of parameters in our model is less than that of the DGPs. Note that [Krauth et al.(2016)Krauth, Bonilla, Cutajar, and Filippone] recently obtained 99.11% accuracy with the AutoGP framework with MNLL 0.033, while our model achieves the lowest MNLL 0.0328 with an accuracy of 99.24%.

A common large-scale data in the GP field is the AIRLINE data set, which contains flight information for 5+

million US flights in 2008. Although this data set is not public, we found a substitute public data set that contains more than 6+ million records of flight information.³ We used this 8-dimensional data set for classification to determine whether a flight has been delayed or not. We constructed the test set using the scripts provided in [Wilson et al.(2016)Wilson, Hu, Salakhutdinov, and Xing], where 100,000 data points were held out for testing. We constructed our models using the 100 RBF-based random features and set the height of trees to one so that it matched the number of parameters in one-hidden layer DGPs [Cutajar et al.(2017)Cutajar, Bonilla, Michiardi, and Filippone]. As shown in Table 4, the results by our model are directly comparable to those obtained by DGPs, which means that the decision tree could almost perform as well as a DGP. Further, when we grow the size of a tree to a height of four, our model achieves 72% accuracy while the counterpart DGP with 10 hidden layers could not converge.

The training time for the MNIST data was 40 minutes, and the training time for the AIRLINE data was 19 minutes.

6 SUMMARY

In this paper, we proposed a novel hierarchical mixture of experts whose inner nodes and experts are both represented by GPs. We chose to work with random features as a way of expanding the GPs. Our GPHMEs outperform all the benchmarks, including tree-structured HMEs and decision trees. They have reduced complexity with respect to other GP-based hierarchical mixtures of experts and offer interpretations of DGPs and deep BNNs. The HMEs have a

3. <https://www.kaggle.com/vikalpdongre/us-flights-data-2008>

limitation in pre-selecting the size, and the number of their parameters increases exponentially. However, it turns out that in practice, we do not need trees with large heights. Our results on various data sets clearly show excellent performance even for large-scale data sets with small trees.

Future work includes the following:

- 1) Pruning of trees. Once the training is completed, one can proceed with pruning the trees. For example, Fig. 2 shows that we might combine the sub-trees which predict the same class. It is important to investigate principled ways of pruning.
- 2) Extensions to ensembles of GPHMEs. Suppose that we have a number of GPHMEs each defined with its own set of feature spaces. Further, let these GPHMEs have prior information that their trees have structures of ISO-N, i.e., Ω is the same across all the nodes, and they have known feature spaces Φ . In that case, the input spaces are projected into different fixed feature spaces rather than random feature spaces. The fixed feature space is easier to interpret than random feature spaces. Therefore, the ensemble of decision trees is naturally an ensemble that exploits known fixed feature spaces. We would like to explore ways of identifying good ensembles, e.g., by allowing the trees to be time-varying, or by spawning new trees from the GPHMEs with good performance using distribution functions of spectral frequencies that are more informative than their respective priors.
- 3) Extension to boosting. This is a rather straightforward task because we only have to replicate the standard boosting routine in constructing a series of trees.
- 4) Modeling experts with DGPs. It might be possible to improve the performance of the GPHMEs by replacing the experts of the tree (the leaves), which are now GPs with DGPs. By doing this we are not losing the nice property of interpretability of the GPHMEs but may gain in performance by using DGPs as experts.
- 5) Feature Selection. A traditional tree can provide information about the most important features of \mathbf{X} . Do our trees also provide information about important features? We plan to examine if information about the importance of features can be extracted from Ω and \mathbf{w} .
- 6) Extension to inducing points approximations. With inducing points, we have an alternative approach to implementing scalable GPs. It will be interesting to examine how trees based on such GPs compare to the ones from this paper.
- 7) Feed forward option. In the paper, we only used feature spaces $\phi(\mathbf{x})$ to make decisions and predictions. However, an interesting direction is to explore the use of the feed-forward option for building the tree, that is, to use both $\phi(\mathbf{x})$ and \mathbf{x} . The objective is not only to improve the accuracy of the tree in its tasks but also to understand how adding the feed-forward option affects the structure of the tree and its parameters.

Table 1
MSEs for regression tasks

	N	D_x	Mean Square Errors				Tree Size			
			GPHME	BHME	Soft	Hard	GPHME	BHME	Soft	Hard
ABA	4177	8	0.405 ± 0.016	0.414 ± 0.014	0.439	0.557	3	15	7	32
ADD	9792	10	0.043 ± 0.001	0.052 ± 0.003	0.094	0.267	3	127	15	202
BOS	506	13	0.112 ± 0.023	0.112 ± 0.020	0.271	0.344	3	15	11	18
CON	1030	8	0.098 ± 0.003	0.147 ± 0.012	0.264	0.286	3	31	13	69

Table 2
Accuracy for binary classification tasks

	N	D_x	Accuracy (%)					Tree Size				
			GPHME	BHME	Soft	C4.5	LDT	GP.	BH.	Soft	C4.5	LDT
BRE	569	30	98.42 ± 00.88	97.47 ± 00.91	95.34	93.80	95.09	3	15	17	47	4
GER	1000	24	76.77 ± 01.42	76.71 ± 01.19	75.74	69.07	74.16	7	7	16	142	7
MAG	19020	10	87.83 ± 00.22	79.25 ± 00.29	81.27	84.09	83.07	7	63	17	1072	40
MUS	6598	167	100.00 ± 00.00	100.00 ± 00.00	92.25	94.62	93.59	3	3	22	202	15
PIM	768	8	78.52 ± 00.96	78.13 ± 01.44	70.85	69.41	76.89	3	15	26	111	5
RIN	7400	20	98.05 ± 00.16	76.71 ± 00.62	88.94	87.54	77.25	7	7	368	354	4
SPA	4601	57	94.85 ± 00.41	92.95 ± 00.48	78.38	90.14	89.86	3	3	22	155	13
TWO	7400	20	98.01 ± 00.24	98.06 ± 00.21	97.92	87.59	98.00	7	3	41	429	3

Table 3
Accuracy for multiple classification tasks

	N	D_x	D_y	Accuracy(%)					Tree Size				
				GPHME	BHME	Soft	C4.5	LDT	GP.	BH.	Soft	C4.5	LDT
BAL	625	4	3	97.80 ± 00.72	90.43 ± 02.40	89.85	61.91	88.46	3	7	10	5	3
CMC	1473	9	3	100.00 ± 00.00	100.00 ± 00.00	52.03	50.00	46.64	3	3	21	24	3
DER	358	34	6	99.17 ± 00.53	98.67 ± 01.13	93.60	94.00	93.92	7	31	11	15	11
ECO	336	7	8	87.86 ± 02.91	88.04 ± 03.37	76.78	77.47	81.39	7	3	10	9	11
GLA	214	10	6	97.50 ± 01.84	94.72 ± 02.97	54.05	56.62	53.37	7	63	11	20	9
OPT	5620	62	10	99.07 ± 00.22	96.95 ± 00.26	90.97	84.85	93.73	7	3	58	120	31
PAG	5473	10	5	97.37 ± 00.29	96.59 ± 00.22	95.70	96.71	94.65	7	3	16	23	29
PEN	10992	16	10	99.54 ± 00.05	95.53 ± 00.46	96.64	92.95	96.60	7	3	54	169	66
SEG	2310	18	7	98.31 ± 00.37	95.35 ± 00.77	93.99	94.48	91.96	7	7	22	41	33
YEA	1484	8	10	61.74 ± 00.73	60.00 ± 01.37	55.82	54.61	56.66	3	7	34	24	22

Table 4
Accuracy for large-scale data sets

	Accuracy		MNLL	
	GPHME	DGP	GPHME	DGP
MNIST8M	99.30%	99.14%	0.0372	0.0454
AIRLINE	71.79%	71.73%	0.5521	0.5510

ACKNOWLEDGMENTS

The authors would like to thank the support of NSF under Award 2212506.

REFERENCES

- [Agrawal and Domke(2021)] Abhinav Agrawal and Justin Domke. Amortized variational inference for simple hierarchical models. In A. Beygelzimer, Y. Dauphin, P. Liang, and J. Wortman Vaughan, editors, *Advances in Neural Information Processing Systems*, 2021.
- [Bishop and Svensén(2012)] Christopher M Bishop and Markus Svensén. Bayesian hierarchical mixtures of experts. *arXiv preprint arXiv:1212.2447*, 2012.
- [Cho and Saul(2009)] Youngmin Cho and Lawrence Saul. Kernel methods for deep learning. *Advances in Neural Information Processing Systems*, 22, 2009.
- [Cutajar et al.(2017)] Cutajar, Bonilla, Michiardi, and Filippone] Kurt Cutajar, Edwin V Bonilla, Pietro Michiardi, and Maurizio Filippone. Random feature expansions for deep Gaussian processes. In *International Conference on Machine Learning*, pages 884–893. PMLR, 2017.
- [Dutordoir et al.(2021)] Dutordoir, Hensman, van der Wilk, Ek, Ghahramani, and Dur Vincent Dutordoir, James Hensman, Mark van der Wilk, Carl Henrik Ek, Zoubin Ghahramani, and Nicolas Durrande. Deep neural networks as point estimates for deep Gaussian processes. *Advances in Neural Information Processing Systems*, 34, 2021.
- [Frosst and Hinton(2017)] Nicholas Frosst and Geoffrey Hinton. Distilling a neural network into a soft decision tree. *arXiv preprint arXiv:1711.09784*, 2017.
- [Gal and Turner(2015)] Yarin Gal and Richard Turner. Improving the Gaussian process sparse spectrum approximation by representing uncertainty in frequency inputs. In *International Conference on Machine Learning*, pages 655–664. PMLR, 2015.
- [Guo and Gelfand(1992)] Heng Guo and Saul B Gelfand. Classification trees with neural network feature extraction. In *Proceedings 1992 IEEE Computer Society Conference on Computer Vision and Pattern Recognition*, pages 183–184. IEEE Computer Society, 1992.

- [Hastie et al.(2009)Hastie, Tibshirani, Friedman, and Friedman] Trevor Hastie, Robert Tibshirani, Jerome H Friedman, and Jerome H Friedman. The Elements of Statistical Learning: Data Mining, Inference, and Prediction, volume 2. Springer, 2009.
- [Hensman et al.(2015)Hensman, Matthews, and Ghahramani] James Hensman, Alexander Matthews, and Zoubin Ghahramani. Scalable variational Gaussian process classification. In Artificial Intelligence and Statistics, pages 351–360. PMLR, 2015.
- [Irsoy et al.(2012)Irsoy, Yildiz, and Alpaydin] Ozan Irsoy, Olcay Taner Yildiz, and Ethem Alpaydin. Soft decision trees. In Proceedings of the 21st International Conference on Pattern Recognition (ICPR2012), pages 1819–1822. IEEE, 2012.
- [Irsoy et al.(2014)Irsoy, Yildiz, and Alpaydin] Ozan Irsoy, Olcay Taner Yildiz, and Ethem Alpaydin. Budding trees. In 2014 22nd international conference on pattern recognition, pages 3582–3587. IEEE, 2014.
- [Jordan and Jacobs(1994)] Michael I Jordan and Robert A Jacobs. Hierarchical mixtures of experts and the EM algorithm. Neural Computation, 6(2):181–214, 1994.
- [Krauth et al.(2016)Krauth, Bonilla, Cutajar, and Filippone] Karl Krauth, Edwin V Bonilla, Kurt Cutajar, and Maurizio Filippone. Autogp: Exploring the capabilities and limitations of Gaussian process models. arXiv preprint arXiv:1610.05392, 2016.
- [Lawrence and Moore(2007)] Neil D Lawrence and Andrew J Moore. Hierarchical Gaussian process latent variable models. In Proceedings of the 24th international Conference on Machine Learning, pages 481–488, 2007.
- [Lázaro-Gredilla et al.(2010)Lázaro-Gredilla, Quinonero-Candela, Rasmussen, and Figueiras-Vidal] Miguel Lázaro-Gredilla, Joaquin Quinonero-Candela, Carl Edward Rasmussen, and Aníbal R Figueiras-Vidal. Sparse spectrum Gaussian process regression. The Journal of Machine Learning Research, 11:1865–1881, 2010.
- [Lee et al.(2017)Lee, Bahri, Novak, Schoenholz, Pennington, and Sohl-Dickstein] Jaehoon Lee, Yasaman Bahri, Roman Novak, Samuel S Schoenholz, Jeffrey Pennington, and Jascha Sohl-Dickstein. Deep neural networks as Gaussian processes. arXiv preprint arXiv:1711.00165, 2017.
- [Loh(2011)] Wei-Yin Loh. Classification and regression trees. Wiley Interdisciplinary Reviews: Data Mining and Knowledge Discovery, 1(1):14–23, 2011.
- [Murthy et al.(1994)Murthy, Kasif, and Salzberg] Sreerama K Murthy, Simon Kasif, and Steven Salzberg. A system for induction of oblique decision trees. Journal of Artificial Intelligence Research, 2:1–32, 1994.
- [Neal(2012)] Radford M Neal. Bayesian Learning for Neural Networks, volume 118. Springer Science & Business Media, 2012.
- [Ng and Deisenroth(2014)] Jun Wei Ng and Marc Peter Deisenroth. Hierarchical mixture-of-experts model for large-scale Gaussian process regression. arXiv preprint arXiv:1412.3078, 2014.
- [Pleiss and Cunningham(2021)] Geoff Pleiss and John P Cunningham. The limitations of large width in neural networks: A deep Gaussian process perspective. Advances in Neural Information Processing Systems, 34, 2021.
- [Quinlan(2014)] J Ross Quinlan. C4. 5: Programs for Machine Learning. Elsevier, 2014.
- [Rahimi and Recht(2007)] Ali Rahimi and Benjamin Recht. Random features for large-scale kernel machines. Advances in neural information processing systems, 20, 2007.
- [Schölkopf(1997)] Bernhard Schölkopf. Support Vector Learning. PhD thesis, Oldenbourg München, Germany, 1997.
- [Shi et al.(2005)Shi, Murray-Smith, and Titterton] Jian Qing Shi, Roderick Murray-Smith, and D Michael Titterton. Hierarchical Gaussian process mixtures for regression. Statistics and Computing, 15(1):31–41, 2005.
- [Simard et al.(2003)Simard, Steinkraus, and Platt] PY Simard, D Steinkraus, and JC Platt. Best practices for convolutional neural networks applied to visual document analysis. In Seventh International Conference on Document Analysis and Recognition, 2003. Proceedings., pages 958–963. IEEE, 2003.
- [Wilson and Izmailov(2020)] Andrew G Wilson and Pavel Izmailov. Bayesian deep learning and a probabilistic perspective of generalization. Advances in Neural Information Processing Systems, 33: 4697–4708, 2020.
- [Wilson et al.(2016)Wilson, Hu, Salakhutdinov, and Xing] Andrew G Wilson, Zhiting Hu, Russ R Salakhutdinov, and Eric P Xing. Stochastic variational deep kernel learning. Advances in Neural Information Processing Systems, 29, 2016.
- [Yildiz and Alpaydin(2001)] CT Yildiz and Ethem Alpaydin. Omnivariate decision trees. IEEE Transactions on Neural Networks, 12(6):1539–1546, 2001.
- [Yildiz and Alpaydin(2005)] Olcay Taner Yildiz and Ethem Alpaydin. Linear discriminant trees. International Journal of Pattern Recognition and Artificial Intelligence, 19(03):323–353, 2005.
- [Yoo and Sael(2021)] Jaemin Yoo and Lee Sael. Gaussian soft decision trees for interpretable feature-based classification. In Pacific-Asia Conference on Knowledge Discovery and Data Mining, pages 143–155. Springer, 2021.